Intraoperative 3D reconstruction of prostate brachytherapy implants with automatic pose correction



2011 Phys. Med. Biol. 56 5011

(http://iopscience.iop.org/0031-9155/56/15/022)

Phys. Med. Biol. **56** (2011) 5011–5027 doi:10.1088/0031-9155/56/15/022

# Intraoperative 3D reconstruction of prostate brachytherapy implants with automatic pose correction

**Junghoon Lee[1], Nathanael Kuo[2], Anton Deguet[3], Ehsan Dehghan[1], Danny Y Song[4], Everette C Burdette[5] and Jerry L Prince[1]**

[1] Department of Electrical and Computer Engineering, Johns Hopkins University, Baltimore, MD 21218, USA
[2] Department of Biomedical Engineering, Johns Hopkins University, Baltimore, MD 21218, USA
[3] Department of Computer Science, Johns Hopkins University, Baltimore, MD 21218, USA
[4] Department of Radiation Oncology and Molecular Radiation Sciences, Johns Hopkins University, Baltimore, MD 21231, USA
[5] Acoustic MedSystems Inc., Champaign, IL 61820, USA

E-mail: junghoon@jhu.edu

Received 14 April 2011, in final form 13 June 2011
Published 19 July 2011
Online at stacks.iop.org/PMB/56/5011

**Abstract**

The success of prostate brachytherapy critically depends on delivering adequate dose to the prostate gland, and the capability of intraoperatively localizing implanted seeds provides potential for dose evaluation and optimization during therapy. REDMAPS is a recently reported algorithm that carries out seed localization by detecting, matching and reconstructing seeds in only a few seconds from three acquired x-ray images (Lee *et al* 2011 *IEEE Trans. Med. Imaging* **29** 38–51). In this paper, we present an automatic pose correction (APC) process that is combined with REDMAPS to allow for both more accurate seed reconstruction and the use of images with relatively large pose errors. APC uses a set of reconstructed seeds as a fiducial and corrects the image pose by minimizing the overall projection error. The seed matching and APC are iteratively computed until a stopping condition is met. Simulations and clinical studies show that APC significantly improves the reconstructions with an overall average matching rate of $\geqslant$99.4%, reconstruction error of $\leqslant$0.5 mm, and the matching solution optimality of $\geqslant$99.8%.

## 1. Introduction

Prostate cancer is a serious health concern in North America. In 2010, there were 217 730 estimated new cases and 32 050 estimated deaths in the United States, which comprises about 28% of all new cancers found in men and 11% of all estimated cancer deaths for men,

  

respectively (Jemal *et al* 2010). The appropriate treatment for prostate cancer depends on whether the cancer is localized to the gland, locally advanced, or spread beyond the gland. Especially if prostate cancer is diagnosed early, it can be treated very effectively with a near 100% 5 year relative survival rate (Jemal *et al* 2010). Low dose rate transperineal brachytherapy has become one of the most popular options for an early-stage organ-confined prostate cancer treatment (Potters 2003), achieving outcomes that are comparable to other treatments such as radical prostatectomy and external-beam radiation therapy while reducing complications and side-effects to the patients (Merrick *et al* 2001, Blasko *et al* 2002, Peschel and Colberg 2003, Cooperberg *et al* 2004, Lee *et al* 2003). It is a minimally invasive procedure, and therefore recovery time is relatively short. In most cases, patients can be discharged the same day of treatment and return to their normal activities within a few days after the treatment. During the procedure, the surgeon permanently implants radioactive seeds ($^{125}$I or $^{103}$Pd) throughout the entire prostate, where the number of implanted seeds (typically 40–130) is determined by the volume of the prostate. The clinical outcome of a brachytherapy procedure critically depends on the ability to treat the target gland with a sufficient therapeutic dose (Potters 2003, Kollmeier *et al* 2003) while minimizing radiation toxicity to adjacent healthy tissues, most notably, the urethra and rectum (Roach 2004, Salem *et al* 2003). Accordingly, achieving an optimal dose distribution is the key to eradicating cancer and minimizing unnecessary toxicity.

In a contemporary brachytherapy procedure, transrectal ultrasound (TRUS) is typically used to guide the implant procedure, because it can visualize the prostate well, is inexpensive, and is real time (Prestidge *et al* 1998). It is, however, not effective for imaging seeds and brachytherapy needles because they are not reliably visible on ultrasound, and needle tracks and calcifications may create echoes similar to those created by seeds. Seed positions are usually estimated and updated intraoperatively at the time of deposition based on the needle tip visualized on longitudinal ultrasound images, which is often called *real-time dosimetry*. However, due to procedural variations caused by patient motion, needle deviation, and soft-tissue deformation including edema, it is difficult to implant seeds at the exact planned locations (Prestidge *et al* 1998, Beyer *et al* 2000, Nag *et al* 2001). Also, real-time dosimetry does not account for these effects occurring during the implant (Waterman *et al* 1998, Chen *et al* 2000, Dawson *et al* 1994, Tanaka *et al* 2007). Fluoroscopy can assist in identification of implanted seed positions, but it is still challenging to identify them relative to the prostate due to the difficulties in visualizing soft tissues using x-rays. As a consequence, intraoperative dosimetric variations are not identified until a postoperative CT scan, and it is sometimes necessary to implant additional seeds to underdosed regions in another implant session which has now become technically more difficult (Davis *et al* 2000, Keyes *et al* 2004). Also, overdosed regions cannot be corrected and this results in unintended consequences of hot spots including increased dose to critical structures and increased risk of toxicity to the patient. To address these limitations of real-time dosimetry, a method that provides the capability to visualize the implanted seeds and to continually adapt to the dynamic character of implants has long been needed. This capability, termed as *dynamic dosimetry*, is specifically identified as desirable and worthy to pursue (Nag *et al* 2001). Therefore, multimodal imaging approaches that combine x-ray and TRUS have been previously proposed to visualize both prostate and seeds and reconstruct seed positions in relation to prostate (Amols and Rosen 1981, Altschuler and Kassaee 1997, Narayanan *et al* 2002, Todor *et al* 2002, Jain *et al* 2005c, Lee *et al* 2009, 2011), thereby permitting intraoperative monitoring and dosimetry modifications.

It is well known that brachytherapy seeds can be reconstructed from at least three x-ray images by resolving seed correspondences between images, provided that every seed is segmented with its 2D image coordinates in every image (Altschuler and Kassaee 1997,

Narayanan *et al* 2002, Todor *et al* 2003, Jain *et al* 2005c, Singh *et al* 2007). Seeds in correspondence can be related to the same physical seed and the seed location can be computed by triangulation. Recent studies further investigated the seed matching problem in order to automatically resolve the so-called *hidden seed problem,* where seeds cannot be reliably identified and localized on the projection images due to a significant amount of overlaps (Lee *et al* 2009, 2011, Tutar *et al* 2003, Lam *et al* 2004, Su *et al* 2004, 2007b, Narayanan *et al* 2004). These algorithms do not require an explicit identification of all the seeds in every image and are able to handle different number of detected seeds in each image. For accurate reconstruction of the implanted seeds from a series of x-ray images, accurate estimation of image poses is critical due to the small size of the brachytherapy seeds. Therefore, many of the previously proposed methods used isocentric x-ray systems such as CT, C-arm CT, and radiation therapy simulators that are equipped with rotational encoders (Altschuler and Kassaee 1997, Narayanan *et al* 2002, 2004, Tutar *et al* 2003, Su *et al* 2004, Kaplan *et al* 2006, Westendorp *et al* 2007). However, since these systems are generally very expensive and require a dedicated interventional suite, they cannot be readily adopted by local hospitals. In addition, the patient should be re-positioned between the treatment and the x-ray image acquisition because he cannot fit into the imaging gantry with the high lithotomy position (the pose used in brachytherapy implantation), causing deformation of the prostate and the seeds between the implantation and the image acquisition. Therefore, recently proposed methods were designed to work with any x-ray imaging system that allows arbitrary source-detector motion, e.g., non-isocentric mobile C-arm that is available in most hospitals (Lee *et al* 2009, 2011, Kon *et al* 2006, Siebert *et al* 2007). The mobile C-arm is useful for intraoperative imaging due to its mobility, easy rotation and translation of the source detector, and relatively smaller system size compared to CT or radiation therapy simulator, thus allowing imaging while the patient is in his surgical position.

The most common tracking systems that are used for intraoperative tracking of x-ray systems are optical trackers, electromagnetic trackers, and tracking fiducials (Phillips *et al* 2004, Zhang *et al* 2004, Tang *et al* 2004, Jain *et al* 2005b, Peters and Cleary 2008). However, tracking an arbitrary motion of the source and detector in an imaging system is not trivial and may add complexity to the procedure. Also, external tracking systems such as optical or electromagnetic trackers are very expensive and have limitations such as the requirement of line-of-sight and interference with an external magnetic field, and also require additional space within the already-crowded operating room (OR). Compared to off-the-shelf tracking systems, radiographic fiducials are cost effective, easy to setup, and take relatively smaller space because they are located within the imaging field of view. However, their tracking performance is sometimes poorer than external tracking systems depending on the quality of image preprocessing such as image distortion correction and feature segmentation. With any tracking method, a seed reconstruction method that is robust to estimated image-pose errors is critical to successful seed localization because it can easily be corrupted by small pose errors due to the small size of the brachytherapy seeds.

A few groups have combined the seed reconstruction with image-pose adjustment using the reconstructed seeds or resolved seed correspondences in an iterative way (Tubic *et al* 2001, Lee *et al* 2009, Dehghan *et al* 2010). However, they require an explicit identification of seeds in every image (Tubic *et al* 2001), accurate initial reconstruction (Tubic *et al* 2001, Lee *et al* 2009), and relatively large number of images (Lee *et al* 2009), and are specifically designed and/or tested for an isocentric x-ray imaging systems (Tubic *et al* 2001, Dehghan *et al* 2010). In addition, all of these methods require repeated reconstructions with the same computational complexity at every iteration, thereby adding a significant amount of computation time.

We have previously proposed an optimal matching algorithm, called REDMAPS, that is able to reconstruct seed positions from three or more x-ray images even when there are a significant number of overlapping seeds in every image (Lee *et al* 2011). Although REDMAPS was proven to be robust to image-pose errors, e.g., up to 2° rotational errors and 5 mm translational errors with over 97.5% average seed matching rate, its performance degrades as pose errors increase. This is not only a problem of REDMAPS, but also of all seed reconstruction algorithms that do not actively correct the image poses during the reconstruction process. In this paper, we describe an automatic pose correction (APC) process that uses a set of reconstructed seeds as a fiducial and automatically corrects the pose errors. The new reconstruction process combines APC and REDMAPS, and iteratively solves the seed matching and the pose correction to improve the overall seed matching rate and the reconstruction errors as well as the optimality of the matching solution. APC-REDMAPS starts with parameters that accommodate relatively large tracking errors, but adaptively change them in successive reconstructions as the image-pose errors are improved by APC, thus requiring much lower computational complexity. APC-REDMAPS was validated on both simulations and clinical data sets, specifically focusing on simulations and data in which REDMAPS alone fails to have acceptable seed detection rates.

## 2. Methods

### *2.1. Image acquisition and preprocessing*

APC-REDMAPS uses three fluoroscopy images to reconstruct implanted seeds. Fluoroscopy images are acquired using a mobile C-arm with an x-ray image intensifier (XRII) detector, and most XRII-based C-arm images show a considerable amount of geometric distortion which shifts the location of the 2D projected seeds and therefore has to be corrected prior to the reconstruction. Additionally, C-arm calibration is necessary to determine intrinsic camera parameters, i.e. pixel size and focal spot. In our approach, C-arm is calibrated only once prior to the surgery by using a calibration fixture (Jain 2007). Since it is known that calibration errors do not critically affect the reconstruction result (Jain *et al* 2005a), we only take a representative image at a vertical pose and estimate the intrinsic camera parameters and the geometric dewarp parameters of the C-arm based on this image.

Although the C-arm is calibrated before the surgery, the C-arm pose must be computed during the patient image acquisition to reconstruct a volume from images taken at arbitrary poses. In order to estimate image poses, we use a fluoroscope tracking fiducial called FTRAC that provides a comparable accuracy to other expensive external tracking devices such as optical or electromagnetic trackers (Jain *et al* 2005b), and is also cost effective. Once an image is acquired, the image distortion is first corrected, and seeds and FTRAC features are automatically segmented in seconds (Kuo *et al* 2010, Lee *et al* 2011). Then, the image pose is computed by using the segmented FTRAC features.

In the current system, this preprocessing (distortion correction, segmentation, and pose estimation) is embedded within the image acquisition pipeline so that 2D image coordinates of the seeds and the image pose are computed as soon as each image is acquired while a technician is rotating the C-arm to the next image acquisition pose. Since three fluoroscopy image acquisition only takes less than a minute and the preprocessing is completed during the image acquisition, total processing time before an APC-REDMAPS reconstruction is just about a minute at most or even less. These segmented seed coordinates and image poses are the input to APC-REDMAPS.

### 2.2. Seed reconstruction

In our previous work (Lee *et al* 2011), we formulated the seed reconstruction as a combinatorial optimization problem. It is well-known that at least three images are required to eliminate ambiguity and reliably reconstruct seeds. When three images are used, the seed reconstruction problem can be formulated as

$$\min_{x_{ijk}} \sum_{i=1}^{N_1} \sum_{j=1}^{N_2} \sum_{k=1}^{N_3} c_{ijk}(\Phi, \mathbf{t}) x_{ijk} \tag{1}$$

$$\begin{aligned} \text{s.t.} \quad & \textstyle\sum_{j=1}^{N_2} \sum_{k=1}^{N_3} x_{ijk} \geqslant 1, \quad \forall i \\ & \textstyle\sum_{i=1}^{N_1} \sum_{k=1}^{N_3} x_{ijk} \geqslant 1, \quad \forall j \\ & \textstyle\sum_{i=1}^{N_1} \sum_{j=1}^{N_2} x_{ijk} \geqslant 1, \quad \forall k \\ & \textstyle\sum_{i=1}^{N_1} \sum_{j=1}^{N_2} \sum_{k=1}^{N_3} x_{ijk} = N \\ & x_{ijk} \in \{0, 1\}, \quad \forall i, j, k \end{aligned} \tag{2}$$

where $N$ is the number of implanted seeds, $N_1, N_2, N_3$ are the numbers of identified seeds by segmentation in images 1, 2, 3, respectively, $c_{ijk}$ is a matching cost for a combination of seeds $i, j, k$ in images 1, 2, 3, respectively, and $x_{ijk}$ is an indicator that is equal to 1 when the combination $\langle i, j, k \rangle$ is chosen in the solution and is zero otherwise. We use *reconstruction accuracy* (RA) (Lee *et al* 2011, Siddon and Chin 1985) as our cost metric, and in this paper, we vary $c_{ijk}$ as a function of C-arm pose, i.e. rotation $\Phi = (\phi_1, \phi_2, \phi_3)$ and translation $\mathbf{t} = (t_1, t_2, t_3)$ in order to jointly optimize the seed correspondence and the C-arm pose. Since $x_{ijk}$ is binary, this combinatorial optimization problem is a binary integer programming (BIP) problem. The inequalities in (2) imply that every seed in every image must be chosen at least once in the solution and also permit more than one assignment to each seed to take hidden seeds into account during the optimization. The equality in (2) guarantees that the total number of combinations chosen in the solution is equal to the number of implanted seeds $N$.

Due to the large number (∼100) of implanted seeds in brachytherapy and the computational complexity of the combinatorial optimization, we first reduce the dimensionality of this optimization by using a pruning algorithm before solving the BIP problem (Lee *et al* 2011, section II-D). Extensive simulations as well as phantom and clinical studies showed that over 99% of the variables in the original BIP problem can be eliminated, and the reduced BIP can be solved by linear programming with relaxed fractional constraints in near real time when the C-arm pose is reasonably estimated (Lee *et al* 2011, section III). If the dimensionality reduction is properly performed, the reduced BIP still contains the globally optimal solution. Therefore, if the solution of the linear programming with relaxed constraints is binary, this solution will be the globally optimal solution of the original BIP problem. However, due to image-pose errors, solutions are not always binary but are sometimes fractional. In this case, we must round the fractional solution to get a binary solution, and this rounded binary solution may no longer be a globally optimal solution. We have shown that about 85% of the REDMAPS solutions with realistic image-pose errors are globally optimal, but this leaves 15% of the solutions that may not be globally optimal (Lee *et al* 2011). Theoretically, when the image poses are accurate with no errors, the minimal RA cost is 0, and the corresponding binary correspondences will be our globally optimal solution. Therefore, by reducing the image-pose error, we have a higher chance to have a globally optimal solution.

### *2.3. Automatic pose correction*

The key idea of dimensionality reduction is that the optimal solution has near-zero cost when the poses of the acquired images are known to be within a small error. However, intraoperative pose tracking of non-encoded mobile C-arm is challenging, and sometimes there is a considerable amount of tracking error. In this case, the underlying assumption of dimensionality reduction may not be valid. Nonetheless, REDMAPS has been shown to correctly recover most of the seed correspondences even when the pose errors are relatively large, e.g., up to 5° rotation and 10 mm translation pose errors (Lee *et al* 2011, figure 4). Therefore, once the initial BIP problem is solved by REDMAPS, most of the seed correspondences are correct, even though the locations of their intersections (and therefore the seed positions) might be inaccurate. We can therefore use the seed correspondences to jointly adjust the C-arm pose and improve the seed matching and positioning in an iterative fashion.

Let ${}^{I}F_{S}$ be the $3 \times 4$ perspective projection matrix from x-ray source frame to the image frame and ${}^{S}F_{W}$ be the $4 \times 4$ transformation between world to x-ray source frames, derived as

$$
\begin{aligned}
{}^{I}F_{S} &= \begin{pmatrix} f/s_x & 0 & o_x & 0 \\ 0 & f/s_y & o_y & 0 \\ 0 & 0 & 1 & 0 \end{pmatrix} \\
{}^{S}F_{W} &= \begin{pmatrix} r_{11} & r_{12} & r_{13} & t_1 \\ r_{21} & r_{22} & r_{23} & t_2 \\ r_{31} & r_{32} & r_{33} & t_3 \\ 0 & 0 & 0 & 1 \end{pmatrix} = \begin{pmatrix} \mathbf{R} & \mathbf{t} \\ \vec{0} & 1 \end{pmatrix}
\end{aligned} \tag{3}
$$

where $f$ is the focal length, $(s_x, s_y)$ is the pixel sampling interval, $(o_x, o_y)$ is the image origin, and the upper-left $3 \times 3$ matrix $\mathbf{R}$ and the upper-right $3 \times 1$ vector $\mathbf{t}$ of ${}^{S}F_{W}$ are the rotation and translation of the x-ray source pose, respectively. Then a $3 \times 4$ projection matrix can be computed as $P(\Phi, \mathbf{t}) = {}^{I}F_{S}\,{}^{S}F_{W}$, and the projected 2D image coordinates $\left(x_i^I(\Phi, \mathbf{t}), y_i^I(\Phi, \mathbf{t})\right)$ of a 3D seed coordinate $\left(x_i^W, y_i^W, z_i^W\right)$ in the world frame is derived as

$$
\begin{aligned}
\begin{pmatrix} x_i^I \\ y_i^I \end{pmatrix} &= \begin{pmatrix} \dfrac{f x_i^S}{s_x z_i^S} + o_x \\ \dfrac{f y_i^S}{s_y z_i^S} + o_y \end{pmatrix} \\
&= \begin{pmatrix} \dfrac{f(r_{11}x_i^W + r_{12}y_i^W + r_{13}z_i^W + t_1)}{s_x(r_{31}x_i^W + r_{32}y_i^W + r_{33}z_i^W + t_3)} + o_x \\ \dfrac{f(r_{21}x_i^W + r_{22}y_i^W + r_{23}z_i^W + t_2)}{s_y(r_{31}x_i^W + r_{32}y_i^W + r_{33}z_i^W + t_3)} + o_y \end{pmatrix}.
\end{aligned} \tag{4}
$$

Since we already know the correspondence between this 3D seed $\left(x_i^W, y_i^W, z_i^W\right)$ and its corresponding 2D segmented seeds $\left(x_i^{\text{seg}}, y_i^{\text{seg}}\right)$, the projection error can be computed as

$$
\Delta\mathbf{x}_i = \begin{pmatrix} \delta x_i(\Phi, \mathbf{t}) \\ \delta y_i(\Phi, \mathbf{t}) \end{pmatrix} = \begin{pmatrix} x_i^I(\Phi, \mathbf{t}) - x_i^{\text{seg}} \\ y_i^I(\Phi, \mathbf{t}) - y_i^{\text{seg}} \end{pmatrix} \tag{5}
$$

and its first-order approximation is

$$\Delta \mathbf{x}_i \approx \begin{pmatrix} \frac{\partial x_i^I}{\partial \phi_1} & \frac{\partial x_i^I}{\partial \phi_2} & \frac{\partial x_i^I}{\partial \phi_3} & \frac{\partial x_i^I}{\partial t_1} & \frac{\partial x_i^I}{\partial t_2} & \frac{\partial x_i^I}{\partial t_3} \\ \frac{\partial y_i^I}{\partial \phi_1} & \frac{\partial y_i^I}{\partial \phi_2} & \frac{\partial y_i^I}{\partial \phi_3} & \frac{\partial y_i^I}{\partial t_1} & \frac{\partial y_i^I}{\partial t_2} & \frac{\partial y_i^I}{\partial t_3} \end{pmatrix} \begin{pmatrix} \Delta\phi_1 \\ \Delta\phi_2 \\ \Delta\phi_3 \\ \Delta t_1 \\ \Delta t_2 \\ \Delta t_3 \end{pmatrix} = \mathbf{J}\Delta\mathbf{E} \tag{6}$$

where $\mathbf{J}$ is the Jacobian and $\Delta\mathbf{E} = (\Delta\phi_1, \Delta\phi_2, \Delta\phi_3, \Delta t_1, \Delta t_2, \Delta t_3)^{\mathrm{t}}$ is the pose error. The Jacobian $\mathbf{J}$ can be explicitly computed in the following way. For rotation

$$\frac{\partial x_i^I}{\partial \phi_j} = \frac{f\left(z_i^S \frac{\partial x_i^S}{\partial \phi_j} - x_i^S \frac{\partial z_i^S}{\partial \phi_j}\right)}{s_x {z_i^S}^2} \tag{7}$$

$$\frac{\partial y_i^I}{\partial \phi_j} = \frac{f\left(z_i^S \frac{\partial y_i^S}{\partial \phi_j} - y_i^S \frac{\partial z_i^S}{\partial \phi_j}\right)}{s_y {z_i^S}^2}, \tag{8}$$

and for translation

$$\frac{\partial x_i^I}{\partial t_1} = \frac{f}{s_x\left(r_{31}x_i^W + r_{32}y_i^W + r_{33}z_i^W + t_3\right)} \tag{9}$$

$$\frac{\partial x_i^I}{\partial t_2} = 0 \tag{10}$$

$$\frac{\partial x_i^I}{\partial t_3} = -\frac{f\left(r_{11}x_i^W + r_{12}y_i^W + r_{13}z_i^W + t_1\right)}{s_x\left(r_{31}x_i^W + r_{32}y_i^W + r_{33}z_i^W + t_3\right)^2} \tag{11}$$

$$\frac{\partial y_i^I}{\partial t_1} = 0 \tag{12}$$

$$\frac{\partial y_i^I}{\partial t_2} = \frac{f}{s_y\left(r_{31}x_i^W + r_{32}y_i^W + r_{33}z_i^W + t_3\right)} \tag{13}$$

$$\frac{\partial y_i^I}{\partial t_3} = -\frac{f\left(r_{21}x_i^W + r_{22}y_i^W + r_{23}z_i^W + t_2\right)}{s_y\left(r_{31}x_i^W + r_{32}y_i^W + r_{33}z_i^W + t_3\right)^2}. \tag{14}$$

Using (6)–(14), we estimate the pose-error $\Delta\mathbf{E}$ using Newton's method (Bertsekas 1999). The current pose $\mathbf{R}_k$ (rotation) and $\mathbf{t}_k$ (translation) are updated using the currently estimated pose error $\Delta\mathbf{E}_k = (\Delta\mathbf{R}_k, \Delta\mathbf{t}_k)$ as follows:

$$\mathbf{R_{k+1}} = \mathbf{R_k}\Delta\mathbf{R_k}, \qquad \mathbf{t_{k+1}} = \mathbf{t_k} + \Delta\mathbf{t_k}. \tag{15}$$

This method has been reported to be more robust and less sensitive to numerical errors than directly updating the rotation angles and translation vector, i.e. $\Phi_{k+1} = \Phi_k + \Delta\Phi_k, \mathbf{t}_{k+1} = \mathbf{t}_k + \Delta\mathbf{t}_k$ (Jain *et al* 2005b). The optimization stops when the mean RA cost difference between successive reconstructions is less than 0.1% of the current RA cost, i.e. $\left(\mathrm{RA}_{k+1}^{\mathrm{mean}} - \mathrm{RA}_k^{\mathrm{mean}}\right)/\mathrm{RA}_k^{\mathrm{mean}} < 0.001$. In simulations, we observed that the optimization converges within 20 iterations in all cases with this stopping condition (see section 3.3), and therefore set the maximum number of iterations to be 50.

The APC process is combined with REDMAPS seed reconstruction and given the name APC-REDMAPS, and the seed matching and the pose correction are iteratively updated until the APC optimization converges. Figure 1 shows the APC-REDMAPS flowchart.

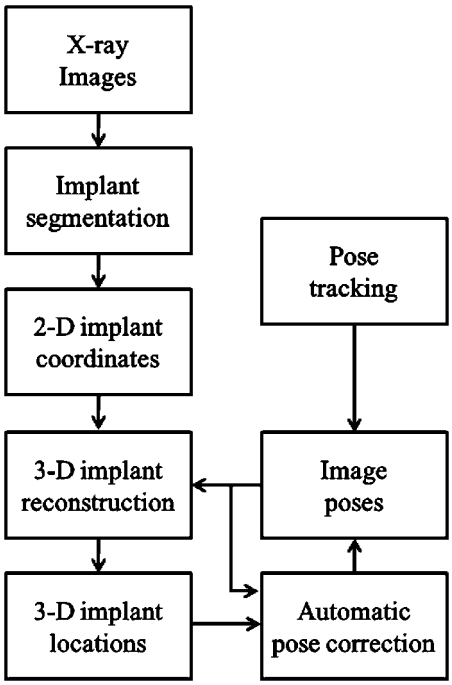


**Figure 1.** APC-REDMAPS flowchart.

### *2.4. Adaptive dimensionality reduction*

When three images are used, the lower bound of RA cost associated with a combination of seeds $\langle i_1, i_2, i_3 \rangle$ can be derived by using lemma II.2 in Lee *et al* (2011) as

$$\mathrm{RA}(i_1, i_2, i_3)^2 \geqslant \frac{1}{12} \sum_{j,k \in \{1,2,3\}, k>j} d(l_{i_j}, l_{i_k})^2 \tag{16}$$

where $d(l_{i_j}, l_{i_k})$ is the Euclidean distance between lines $l_{i_j}$ and $l_{i_k}$ that originate from seeds $i_j$ and $i_k$ in images $j$ and $k$, respectively. Therefore, we set a dimensionality reduction threshold $\eta$, and eliminate infeasible combinations that yield $\mathrm{RA}(i_1, i_2, i_3)^2 \geqslant 1/12 \sum_{j,k \in \{1,2,3\}, k>j} d(l_{i_j}, l_{i_k})^2 > \eta$ from further consideration in the reduced BIP problem.

As the APC process improves the C-arm pose, $\eta$ can be adaptively reduced because more accurate image poses result in smaller RA cost. Therefore, for every iteration, we change $\eta$ by $\eta = s \times \max c_{ijk}$ for $\{i, j, k | x_{ijk} = 1\}$ where $s$ is set to be 2 in this paper. By adaptively reducing $\eta$, we can achieve larger dimensionality reduction and reduced computation time in successive iterations. At the same time, this process is much faster than use of a lesser dimensionality reduction factor and still has a high probability of yielding a binary solution that is globally optimal.

## 3. Results and discussion

### *3.1. Simulations*

We first evaluated APC-REDMAPS on varying levels of simulated pose errors. In our previous study (Lee *et al* 2011), REDMAPS was shown to be robust to errors in seed segmentation

and intrinsic camera calibration errors (i.e. focal length and image origin). Therefore, our simulations here were focused on the robustness of APC-REDMAPS to rotational and translational pose errors which are the two major errors that affect reconstruction results.

We considered a nominal 50 cc prostate with four different seed densities varying from 1.0 to 2.5 seeds/cc with 0.5 seeds/cc increments, resulting in $N = \{54, 72, 96, 128\}$ implanted seeds. Each seed was modeled as a cylinder that is 1.45 mm in length and 0.8 mm in diameter to create a similar x-ray projection image of a $^{103}$Pd seed. We assumed that x-ray projections were acquired using a C-arm with a focal length of 1000 mm and image pixel size of $0.44 \times 0.44$ mm$^2$. For each seed density, we generated 30 data sets, and created three projections on a 20° cone around the AP-axis in each data set. In every image, 3.2% on average and up to 11.7% of the seeds were hidden. We added varying levels of pose errors that were randomly generated from a uniform distribution on $[-h, h]$ to the known rotation and translation. Rotational pose error varied from $h = 0°$–$5°$ with 1° increment, and translational pose error varied from $h = 0$–12 mm with 2 mm steps. The dimensionality reduction threshold was initially set as $\eta = 9$ so that any combination that yields RA cost larger than 3 mm was rejected (see (16)), and was adaptively reduced as the iterations progressed. Above 5° rotational and 12 mm translational pose errors, REDMAPS often failed to find the seed correspondence with this initial threshold, in which case we could not process APC. Larger pose errors can be handled by increasing the initial dimensionality reduction threshold, but, in turn, it will reduce the amount of dimensionality reduction and increase the computation time at the first several iterations. A total of 720 (4 seed densities × 30 data sets × 6 rotational error levels) and 840 (4 seed densities × 30 data sets × 7 translational error levels) reconstructions were computed for rotational and translational pose errors, respectively, using both REDMAPS and APC-REDMAPS.

The reconstruction results are plotted in figure 2. In comparison to REDMAPS, APC-REDMAPS improves the reconstruction results in every aspect; seed matching rate, reconstruction error and optimality of the solution. Even when the initial seed matching rate is about 70%, APC-REDMAPS almost perfectly recovered the seed correspondences. In order to evaluate the RA, we compared the reconstructed seeds with the ground truth seed locations. The reconstructed seeds could be systematically rotated or shifted in the APC-REDMAPS reconstruction because we corrected all three poses. However, since reconstructed seeds will be registered to the TRUS prostate volume and the dose field will be computed based on the registered seed cloud, these systematic rotation and translation will not affect the final dosimetry. Therefore, we computed relative reconstruction errors of the matched seeds in order to assess the RA after performing rigid point-cloud (reconstruction) to point-cloud (ground truth) registration (Horn 1987, Besl and McKay 1992). The reconstruction errors were always less than 0.05 mm as shown in figures 2(c) and (d). By adjusting the image poses, we could significantly improve the optimality of the solution. In all cases, the resulting solutions of APC-REDMAPS were binary and therefore globally optimal.

### *3.2. Clinical study*

APC-REDMAPS was evaluated on 15 patient data sets that were collected under IRB-approved protocols at Johns Hopkins Hospital. For all patients, $^{103}$Pd seeds (Theragenics®, GA, United States) were implanted. For each patient data set, we acquired six to nine images within 20° cone around the AP-axis, and each image pose was tracked by using FTRAC. From among the collected images, we selected six to nine images that were not acquired at the same pose and their poses could be estimated well using FTRAC. We then computed 958 reconstructions using all possible combinations of three images. For ground truth, we selected

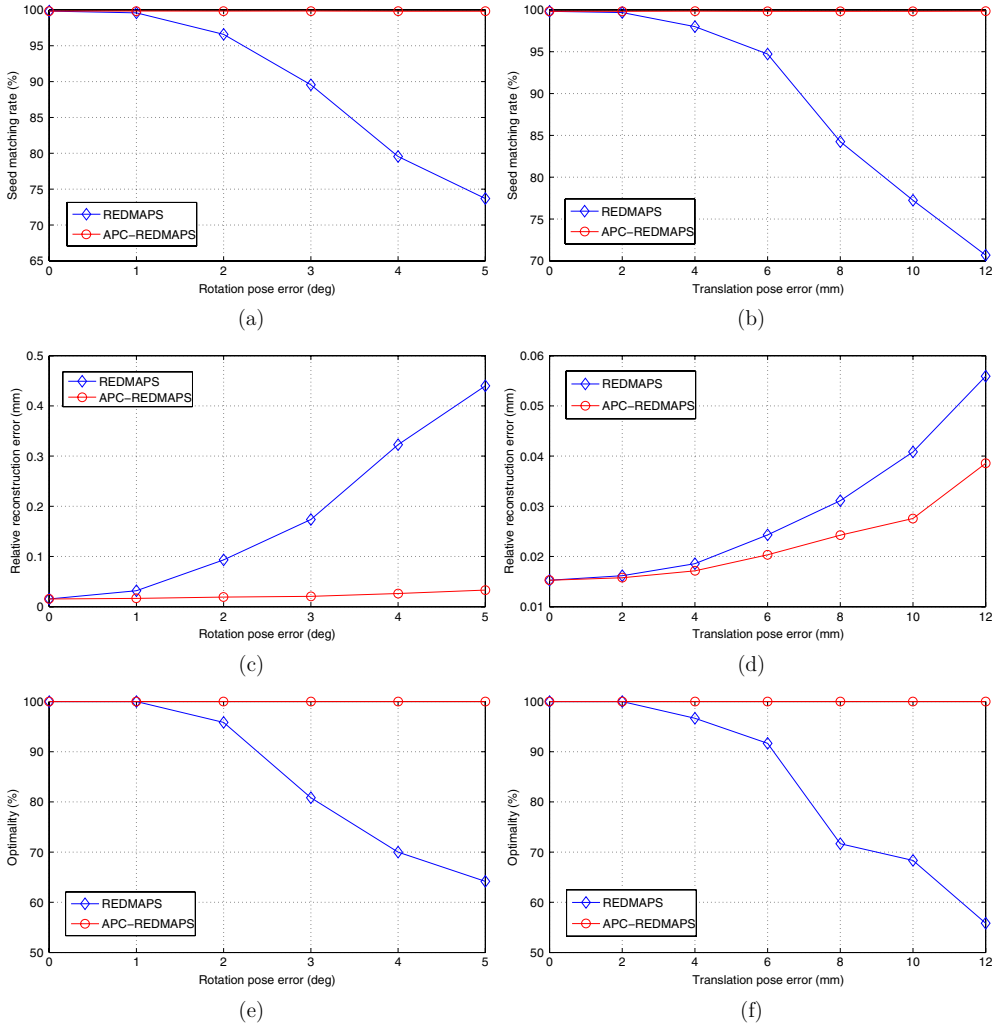


**Figure 2.** Simulation results. Performance comparison between REDMAPS and APC-REDMAPS. (a, b) Seed matching rate, (c, d) relative reconstruction error, and (e, f) solution optimality. We considered different levels of (a, c, e) rotation and (b, d, f) translation pose errors.

five to six images with the smallest residual pose errors (computed using FTRAC software), visually validated and manually corrected the automatic seed segmentations, and reconstructed seeds using REDMAPS. Since more images yield better reconstructions in general (Lee *et al* 2011) and there are no ground truth seed positions for the clinical cases, we used the REDMAPS reconstruction from these five to six images as our ground truth. We compared all reconstructions to the ground truth and computed the seed matching rate, the relative reconstruction error of the correctly matched seeds, and the optimality of the solution.

The results are summarized in table 1. When the angular separations of the images were very small, e.g., $1^\circ - 2^\circ$, REDMAPS could not recover the initial seed correspondences correctly. In addition, relatively large pose errors in some images due to patient motion during image acquisition, missing features of FTRAC in the projection, and/or relatively

**Table 1.** Clinical study results. C-arm poses were computed by using FTRAC. Average seed matching rate, average relative reconstruction error (mean ± std) of the matched seeds and optimality of the solution were computed.

| | | | REDMAPS | | | APC-REDMAPS | | |
|---|---|---|---|---|---|---|---|---|
| Patient ID | Number of seeds | Number of reconstructions | Matching rate (%) | Reconstruction error (mm) | Optimality (% ) | Matching rate (% ) | Reconstruction error (mm) | Optimality (%) |
| 1 | 78 | 20 | 93.3 | $0.6 \pm 0.3$ | 80.0 | 99.6 | $0.5 \pm 0.2$ | 100 |
| 2 | 66 | 84 | 99.1 | $0.4 \pm 0.1$ | 96.4 | 100.0 | $0.3 \pm 0.1$ | 100 |
| 3 | 84 | 84 | 87.7 | $0.7 \pm 0.4$ | 59.5 | 99.4 | $0.4 \pm 0.1$ | 100 |
| 4 | 70 | 56 | 96.4 | $0.7 \pm 0.3$ | 89.3 | 99.4 | $0.7 \pm 0.3$ | 100 |
| 5 | 77 | 56 | 92.3 | $0.5 \pm 0.3$ | 76.8 | 99.9 | $0.4 \pm 0.1$ | 100 |
| 6 | 53 | 84 | 94.0 | $0.7 \pm 0.3$ | 91.7 | 98.9 | $0.7 \pm 0.3$ | 98.8 |
| 7 | 66 | 84 | 98.3 | $0.4 \pm 0.2$ | 95.2 | 99.9 | $0.4 \pm 0.2$ | 100 |
| 8 | 81 | 56 | 97.1 | $0.4 \pm 0.1$ | 89.3 | 99.0 | $0.5 \pm 0.1$ | 100 |
| 9 | 75 | 84 | 79.6 | $0.9 \pm 0.4$ | 51.2 | 98.6 | $0.4 \pm 0.1$ | 100 |
| 10 | 90 | 35 | 88.5 | $0.6 \pm 0.3$ | 60.0 | 99.9 | $0.4 \pm 0.1$ | 100 |
| 11 | 64 | 35 | 84.3 | $0.9 \pm 0.6$ | 77.1 | 98.8 | $0.6 \pm 0.2$ | 100 |
| 12 | 83 | 84 | 97.5 | $0.4 \pm 0.1$ | 91.7 | 100.0 | $0.4 \pm 0.1$ | 100 |
| 13 | 105 | 84 | 81.8 | $0.9 \pm 0.6$ | 51.2 | 99.5 | $0.5 \pm 0.2$ | 100 |
| 14 | 91 | 56 | 70.4 | $1.4 \pm 0.7$ | 33.9 | 98.7 | $1.0 \pm 0.3$ | 98.2 |
| 15 | 73 | 56 | 88.3 | $0.7 \pm 0.4$ | 53.6 | 99.9 | $0.4 \pm 0.2$ | 100 |
| Overall | | | 90.2 | $0.7 \pm 0.4$ | 74.0 | 99.4 | $0.5 \pm 0.2$ | 99.8 |

large segmentation errors caused lower seed matching rate and solution optimality, and higher reconstruction error. For example, for the patient 14, significant patient motions were introduced between image acquisitions, causing relatively lower seed-matching rate and solution optimality, and larger reconstruction errors. For this patient data, the ground truth seed locations were less accurate than other cases, showing significant deviations of the reprojected ground truth seeds from the segmented seeds in every image (note that the ground truth seed locations were computed from five-six images without APC). However, after the APC was performed, APC-REDMAPS was able to achieve an overall seed matching rate of 99.4% with a solution optimality of 99.8%, and an average relative reconstruction error of 0.5 mm.

An example is shown in figure 3. In this case, due to relatively large pose estimation error and very small angular separation between images, REDMAPS could recover only 64.3% of the seed correspondences correctly with an average reconstruction error of 1.4 mm for the matched seeds. However, after the APC process, the seed matching rate increased to 98.8% and the average reconstruction error was reduced to 0.6 mm. It has been reported that 95% or more seeds need to be localized in order to provide an accurate estimation of dose parameters for contemporary $^{125}$I permanent prostate brachytherapy (Su *et al* 2005), and less than 5% deviation of prostate D90 (minimum radiation dose received by 90% of the prostate) can be expected when the seed localization uncertainty is 2 mm (Su *et al* 2007a). Although the activity of a $^{103}$Pd seed that is used in our experiments is not identical to that of an $^{125}$I seed, we expect that a similar accuracy would be clinically acceptable. However, considering the fact that there are about 100 implanted seeds and higher seed detection rate will result in more accurate dose computation, our goal is to achieve over 98% seed detection rate with sub-mm reconstruction error. APC-REDMAPS achieved this accuracy even in the worst case, and significantly improved the overall reconstruction quality compared to REDMAPS.

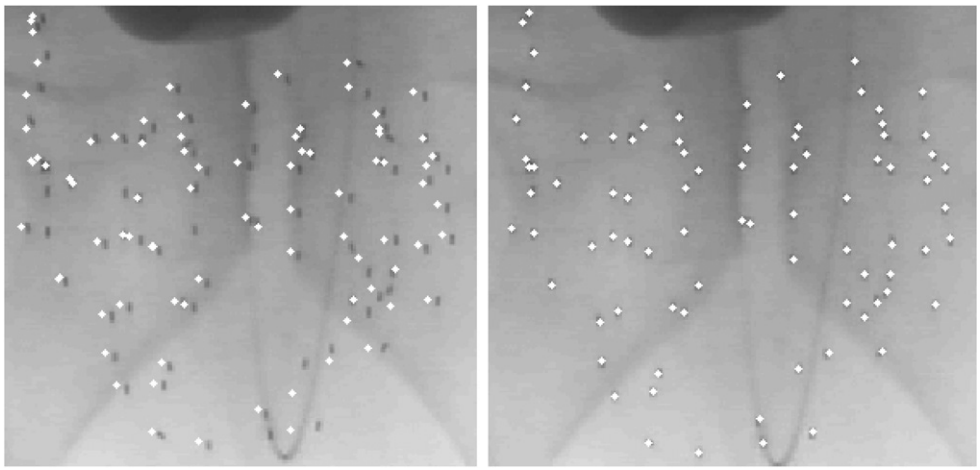

**Figure 3.** Example images of reconstruction results on a clinical data set. The reconstructed seeds are reprojected onto one of the three images (white dots) used for reconstruction. The left image shows one of the worst REDMAPS reconstruction caused by large image-pose errors and small image acquisition angle separation. The pose errors were compensated and the seeds were reconstructed correctly by APC-REDMAPS (right image).

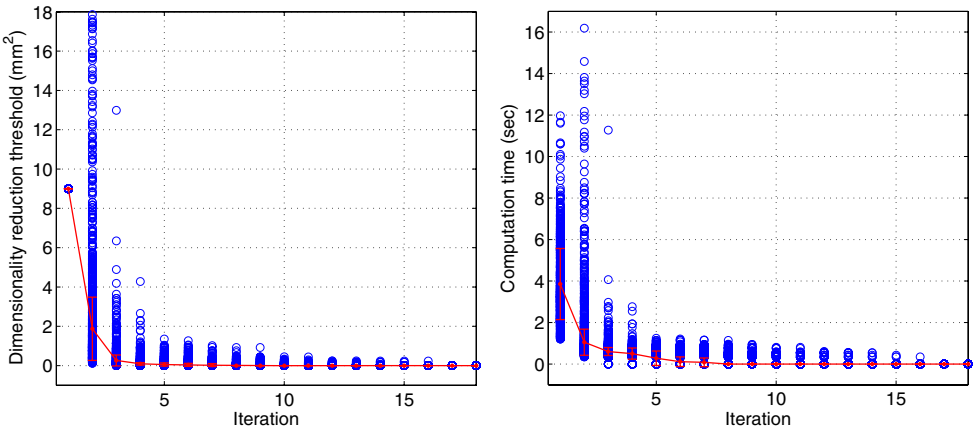


**Figure 4.** Dimensionality reduction threshold (left) and the computation time (right) plots at each iteration. Circles indicate individual measurements at each iteration, and the lines show the mean±std variations.

### *3.3. Dimensionality reduction and processing time*

Since APC-REDMAPS requires multiple seed reconstructions as well as pose corrections, it adds additional processing time to the seed reconstruction process. However, since we adaptively adjust the dimensionality reduction threshold in the successive reconstructions, we can achieve larger dimensionality reduction as the image poses become more accurate. For the 15 patient data sets used in the clinical study, we measured the dimensionality reduction threshold and the processing time at each iteration to see how much additional time we needed for the APC-REDMAPS. As shown in figure 4, the dimensionality reduction threshold is reduced quite rapidly within the first several iterations and the APC-REDMAPS adds only a small amount of time to the initial REDMAPS reconstructions. On average, the

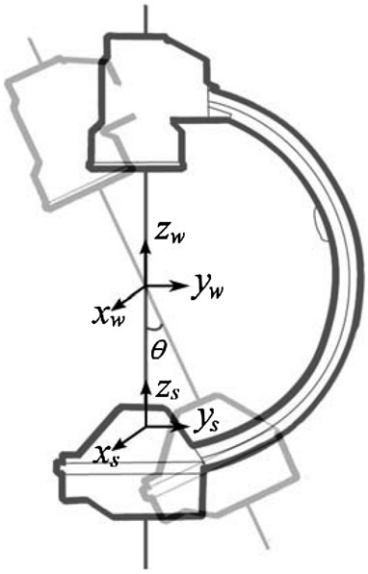


**Figure 5.** Image acquisition geometry for the seed reconstruction without an external tracker.

initial REDMAPS reconstructions took 3.8 s and the APC-REMDAPS added only 2.4 s, thus requiring 6.2 s for the total computation on a PC with a 2.5 GHz CPU. Note that three fluoroscopy image acquisition along with the preprocessing takes about a minute or less and APC-REDMAPS adds about 6 s on average, therefore total processing time from image acquisition to reconstruction is about a minute. Since the final $\eta$ is very small (less than 0.5 mm$^2$ on average), the RA costs of the remaining feasible solutions are very close to 0, thus yielding near 100% solution optimality.

### *3.4. Seed reconstruction without tracking device*

Since APC-REDMAPS can compensate for a significant amount of pose error, we tried to reconstruct the implanted seeds without a tracking device or image-based fiducial. Although mobile C-arms in most hospitals are not isocentric, a small rotation, e.g., 20°, along the C-arc can be considered as roughly isocentric. Therefore, as a rough initialization, the C-arm was assumed to be isocentric, and three images were acquired at three different rotational positions, one AP-view and two oblique views, by rotating the C-arm along the C-arc. The source to (virtual) isocenter distance (SID) is either known from the system specification or can be easily estimated through a calibration process. We assumed that our reference frame is aligned to the source frame at the AP-view and is placed at the virtual isocenter as shown in figure 5. This coordinate choice is preferable because the source frame at AP-view is already (roughly) aligned to the template coordinates, thus providing reasonably good orientation initialization for the TRUS-fluoroscopy registration. Based on this simple geometry, three image poses can be derived as

$$ {}^{S}F_{W}^{i} = \begin{pmatrix} 1 & 0 & 0 & 0 \\ 0 & \cos\theta_i & \sin\theta_i & 0 \\ 0 & -\sin\theta_i & \cos\theta_i & \mathrm{SID} \\ 0 & 0 & 0 & 1 \end{pmatrix}, \qquad i = 1, 2, 3 \tag{17} $$

where ${}^{S}F_{W}^{i}$ is the $i$th image pose.

**Table 2.** Clinical study results without a tracking device. Seed matching rate, relative reconstruction error (mean ± std) of the matched seeds, and optimality of the solution were computed.

| Patient ID | Number of seeds | Number of matched seeds | Matching rate (%) | Reconstruction error (mm) | Optimality |
|---|---|---|---|---|---|
| 12 | 83 | 83 | 100 | $0.4 \pm 0.3$ | Yes |
| 13 | 105 | 104 | 99.1 | $0.7 \pm 0.3$ | Yes |
| 14 | 91 | 90 | 98.9 | $1.0 \pm 0.3$ | Yes |
| 15 | 73 | 73 | 100 | $0.3 \pm 0.3$ | Yes |
| Overall | | | 99.5 | $0.6 \pm 0.4$ | |

Among 15 patients studied in section 3.2, we collected additional data sets for the last four patients using this scenario and no tracking device. Three images were acquired at $\sim 0^\circ$ (AP-view) and $\sim \pm 10^\circ$ (two oblique views) by reading the angular mark on the C-arm, thus providing an initial guess for the $\theta_2$ and $\theta_3$ (note that $\theta_1 = 0$). Due to the inaccuracies of both initially estimated image acquisition angles and our assumption on isocentricity, we decided to compute nine initial REDMAPS reconstructions assuming the oblique views were at the following angles $\pm\{9^\circ, 10^\circ, 11^\circ\}$, and considering all combinations of three images (without applying APC). Since better seed matching yields smaller overall matching cost, we chose the best initial match by comparing the overall seed-matching (RA) costs of these trial reconstructions. Once the best initial condition was automatically determined in this way, APC-REDMAPS was used to iteratively correct the pose (all six degrees of freedom) and improve the reconstruction until convergence. The reconstructed seed locations were compared to the ground truth seed locations. Since we did not know the correspondences between the reconstructed seeds and the ground truth seeds, we computed the seed correspondences by using the iterative closest point (ICP) algorithm (Zhang 1994) and decided that the seed pairs with Euclidean distance larger than 2 mm were not matched.

Table 2 shows the reconstruction results. Even with a rough initialization without using an external tracking device, APC-REDMAPS shows a similar performance to those with FTRAC. Both individual and the overall results are comparable to the corresponding results shown in table 1.

## 4. Conclusions

This paper presents a new algorithm that combines an existing algorithm, REDMAPS, with a new pose correction step for accurate reconstruction and localization of the implanted brachytherapy seeds from a small number of x-ray images. By using the reconstructed seeds with revealed seed correspondences as a fiducial, APC iteratively minimizes the RA cost and improves the estimated image poses. As the RA cost becomes smaller at each iteration, the dimensionality reduction threshold in REDMAPS is adaptively reduced to achieve larger dimensionality reduction and allow faster computation in the BIP optimization. Both simulations and clinical studies show very promising results where we can achieve almost perfect seed detection rate with very small reconstruction error even when the image-pose errors are very large. Especially, as the pose errors are reduced, the resulting solutions become typically binary (on average 99.8% of the solutions were binary in our clinical studies) even under the relaxed fractional constraints, and are therefore globally optimal.

We have also demonstrated a seed reconstruction scenario without using a tracking device. Even when no tracking device was used and the initial pose was roughly estimated under a simplified geometry, APC-REDMAPS was still able to recover image poses and achieve near perfect seed detection rate. Although we relied on the angular mark readings on the C-arm for the initial poses, the results on clinical data sets showed that APC-REDMAPS can accommodate very rough initial guess on the image poses and has a potential for a trackerless seed reconstruction system. As long as we can have initial poses within a very generous margin, e.g., $\sim 5^{\circ}$ and $\sim 10$ mm, APC-REDMAPS can recover image poses and find the seed locations accurately. Also, a multiple initial reconstruction strategy can also be adopted in order to guarantee more accurate initialization.

Overall, the proposed APC in combination with REDMAPS can greatly improve the seed detection rate even from the already good performance of REDMAPS without requiring a significant amount of additional time. This approach not only allows a more generous choice of tracking methods, but also opens a possibility to completely remove the use of any external trackers.

## Acknowledgments

This research was supported in part by the National Institutes of Health/National Cancer Institute (NIH/NCI) under grant 2R44CA099374 and grant 1R01CA151395, and in part by the Department of Defense (DoD) under grant W81XWH-05-1-0407.

## References

Altschuler M D and Kassaee A 1997 Automated matching of corresponding seed images of three simulator radiographs to allow 3D triangulation of implanted seeds *Phys. Med. Biol.* **42** 293–302

Amols H I and Rosen I I 1981 A three-film technique for reconstruction of radioactive seed implants *Med. Phys.* **8** 210–4

Bertsekas D P 1999 *Nonlinear Programming* 2nd edn (Belmont, MA: Athena Scientific)

Besl P J and McKay N D 1992 A method for registration of 3-D shapes *IEEE Trans. Pattern Anal. Mach. Intell.* **14** 239–56

Beyer D C, Shapiro R H and Puente F 2000 Real-time optimized intraoperative dosimetry for prostate brachytherapy: a pilot study *Int. J. Radiat. Oncol. Biol. Phys.* **48** 1583–9

Blasko J, Mate T, Sylvester J, Grimm P and Cavanagh W 2002 Brachytherapy for carcinoma of the prostate: techniques, patient selection, and clinical outcomes *Semin. Radiat. Oncol.* **12** 81–94

Chen Z, Yue N, Wang X, Roberts K B, Peschel R and Nath R 2000 Dosimetric effects of edema in permanent prostate seed implants: a rigorous solution *Int. J. Radiat. Oncol. Biol. Phys.* **47** 1405–19

Cooperberg M R, Broering J M, Litwin M S, Lubeck D P, Mehta S S, Henning J M, Carroll P R and investigators T C 2004 The contemporary management of prostate cancer in the united states: lessons from the cancer of the prostate strategic urologic research eneavor (capsure), a national disease registry *J. Urol.* **171** 1393–401

Davis B J, Herman M G, LaJoie W N, King B F, Kofler J M, Hadaway M A, Wilson T M and Pisansky T M 2000 Supplemental implantation for suboptimal permanent prostate brachytherapy: a prostate phantom study *Radiother. Oncol.* **55S** 91–2

Dawson J E, Wua T, Roya T, Gua J Y and Kim H 1994 Dose effects of seeds placement deviations from pre-planned positions in ultrasound guided prostate implants *Radiother. Oncol.* **32** 268–70

Dehghan E, Lee J, Moradi M, Wen X, Fichtinger G and Salcudean S E 2010 Prostate brachytherapy seed reconstruction using c-arm rotation measurement and motion compensation *Lecture Notes Comput. Sci.* **6361** 283–90

Horn B K P 1987 Closed form solution of absolute orientation using unit quaternions *J. Opt. Soc. Am.* A **4** 629–42

Jain A K 2007 Computation of 3D implant coordinates for prostate brachytherapy *PhD Thesis* Johns Hopkins University Baltimore, Maryland, USA

Jain A K, Kon R, Zhou Y and Fichtinger G 2005a C-arm calibration—is it really necessary? *Proc. MICCAI: LNCS* vol 3749 pp 639–46

Jain A K, Mustafa T, Zhou Y, Burdette C, Chirikjian G S and Fichtinger G 2005b FTRAC—a robust fluoroscope tracking fiducial *Med. Phys.* **32** 3185–98

Jain A K, Zhou Y, Mustafa T, Burdette E C, Chirikjian G S and Fichtinger G 2005c Matching and reconstruction of brachytherapy seeds using the hungarian algorithm (MARSHAL) *Med. Phys.* **32** 3475–92

Jemal A, Siegel R, Xu J and Ward E 2010 Cancer statistics *Cancer J. Clin.* **60** 277–300

Kaplan I D, Meskell P, Oldenburg N E, Saltzman B, Kearney G P and Holupka E J 2006 Real-time computed tomography dosimetry during ultrasound-guided brachytherapy for prostate cancer *Brachytherapy* **5** 147–51

Keyes M, Pickles T, Agranovich A, Kwan W and Morris W J 2004 1251 reimplantation in patients with poor initial dosimetry after prostate brachytherapy *Int. J. Radiat. Oncol. Biol. Phys.* **60** 40–50

Kollmeier M A, Stock R G and Stone N 2003 Biochemical outcomes after prostate brachytherapy with 5-year minimal follow-up: importance of patient selection and implant quality *Int. J. Radiat. Oncol. Biol. Phys.* **57** 645–53

Kon R, Jain A and Fichtinger G 2006 Hidden seed reconstruction from C-arm images in brachytherapy *Proc. IEEE Int. Symp. Biomed. Imag.* pp 526–9

Kuo N, Lee J, Deguet A, Song D Y, Burdette E C and Prince J L 2010 Automatic segmentation of seeds and fluoroscope tracking (FTRAC) fiducial in prostate brachytherapy x-ray images *Proc. SPIE Med. Imaging* **7625** 76252T

Lam S T, Cho P S, MarksII R J and Narayanan S 2004 Three-dimensional seed reconstruction for prostate brachytherapy using Hough trajectories *Phys. Med. Biol.* **49** 557–69

Lee J, Labat C, Jain A K, Song D Y, Burdette E C, Fichtinger G and Prince J L 2011 REDMAPS: reduced-dimensionality matching for prostate brachytherapy seed reconstruction *IEEE Trans. Med. Imaging* **29** 38–51

Lee J, Liu X, Jain A K, Song D Y, Burdette E C, Prince J L and Fichtinger G 2009 Prostate brachytherapy seed reconstruction with Gaussian blurring and optimal coverage cost *IEEE Trans. Med. Imaging* **28** 1955–68

Lee W R, Moughan J, Owen J B and Zelefsky M J 2003 The 1999 patterns of care study of radiotherapy in localized prostate carcinoma: a comprehensive survey of prostate brachytherapy in the united states *Cancer* **98** 1393–401

Merrick G, Butler W, Lief J and Dorsey A 2001 Is brachytherapy comparable with radical prostatectomy and external-beam radiation for clinically localized prostate cancer? *Tech. Urol.* **7** 12–9

Nag S, Ciezki J, Cormack R, Doggett S, DeWyngaert K, Edmundson G, Stock R, Stone N, Yu Y and Zelefsky M 2001 Intraoperative planning and evaluation of permanent prostate brachytherapy *Int. J. Radiat. Oncol. Biol. Phys.* **51** 1422–30

Narayanan S, Cho P and Marks R 2002 Fast cross-projection algorithm for reconstruction of seeds in prostate brachytherapy *Med. Phys.* **29** 1572–9

Narayanan S, Cho P S and Marks R J II 2004 Three-dimensional seed reconstruction from an incomplete data set for prostate brachytherapy *Phys. Med. Biol.* **49** 3483–94

Peschel R and Colberg J 2003 Surgery, brachytherapy, and external-beam radiotherapy for early prostate cancer *Lancet Oncol.* **4** 233–41

Peters T and Cleary K 2008 *Image-Guided Interventions: Technology and Applications* (Heidelberg: Springer)

Phillips R, Mohsen A, Wiant W, Malek S, Li Q, Shah N, Bielby M and Sherman K 2004 *Lecture Notes Comp. Sci.* **3217** 621–8

Potters L 2003 Permanent prostate brachytherapy in men with clinically localised prostate cancer *Clin. Oncol.* **15** 301–15

Prestidge B R, Prete J J, Buchholz T A, Friedland J L, Stock R G, Grimm P D and Bice W S 1998 A survey of current clinical practice of permanent prostate brachytherapy in the United States *Int. J. Radiat. Oncol. Biol. Phys.* **40** 461–5

Roach M I 2004 Reducing the toxicity associated with the use of radiotherapy in men with localized prostate cancer *Urol. Clin. North Am.* **31** 353–66

Salem N, Simonian-Sauvea M, Rosellob R, Alzieua C, Gravisb G, Maraninchic D and Bladou F 2003 Predictive factors of acute urinary morbidity after iodine-125 brachytherapy for localised prostate cancer: a phase 2 study *Radiother. Oncol.* **66** 159–65

Siddon R L and Chin L M 1985 Two-film brachytherapy reconstruction algorithm *Med. Phys.* **12** 77–83

Siebert F A, Srivastav A, Kliemann L, Fohlin H and Kovacs G 2007 Three-dimensional reconstruction of seed implants by randomized rounding and visual evaluation *Med. Phys.* **34** 967–75

Singh V, Mukherjee L, Xu J, Hoffmann K R, Dinu P M and Podgorsak M 2007 Brachytherapy seed localization using geometric and linear programming technique *IEEE Trans. Med. Imaging* **26** 1291–304

Su Y, Davis B J, Furutani K M, Herman M G and Robb R A 2007a Dosimetry accuracy as a function of seed localization uncertainty in permanent prostate brachytherapy: increased seed number correlates with less variability in prostate dosimetry *Phys. Med. Biol.* **52** 3105–19

Su Y, Davis B J, Furutani K M, Herman M G and Robb R A 2007b Prostate brachytherapy seed reconstruction using adaptive grouping technique *Med. Phys.* **34** 2975–84

Su Y, Davis B J, Herman M G and Robb R A 2004 Prostate brachytherapy seed localization by analysis of multiple projections: identifying and addressing the seed overlap problem *Med. Phys.* **31** 1277–87

Su Y, Davis D J, Herman M G, Manduca A and Robb R A 2005 Examination of dosimetry accuracy as a function of seed detection rate in permanent prostate brachytherapy *Med. Phys.* **32** 3049–56

Tanaka O, Hayashi S, Matsuo M, Nakano M, Uno H, Ohtakara K, Miyoshi T, Deguchi T and Hoshi H 2007 Effect of edema on postimplant dosimetry in prostate brachytherapy using CT/MRI fusion *Int. J. Radiat. Oncol. Biol. Phys.* **69** 614–8

Tang T S Y, MacIntyre N J, Gill H S, Fellows R A, Hill N A, Wilson D R and Ellis R E 2004 Accurate assessment of patellar tracking using fiducial and intensity-based fluoroscopic techniques *Med. Image Anal.* **8** 343–51

Todor D A, Cohen G N, Amols H I and Zaider M 2002 Operator-free, film-based 3D seed reconstruction in brachytherapy *Phys. Med. Biol.* **47** 2031–48

Todor D, Zaider M, Cohen G, Worman M and Zelefsky M 2003 Intraoperative dynamic dosimetry for prostate implants *Phys. Med. Biol.* **48** 1153–71

Tubic D, Zaccarin A, Beaulieu L and Pouliot J 2001 Automated seed detection and three-dimensional reconstruction: II. Reconstruction of permanent prostate implants using simulated annealing *Med. Phys.* **28** 2272–9

Tutar I B, Managuli R, Shamdasani V, Cho P S, Pathak S D and Kim Y 2003 Tomosynthesis-based localization of radioactive seeds in prostate brachytherapy *Med. Phys.* **30** 101–9

Waterman F M, Yue N, Corn B W and Dicker A P 1998 Edema associated with i-125 or pd-103 prostate brachytherapy and its impact on post-implant dosimetry: an analysis based on serial CT acquisition *Int. J. Radiat. Oncol. Biol. Phys.* **41** 1069–77

Westendorp H, Hoekstra C J, Riet A, Minken A W and Immerzeel J J 2007 Intraoperative adaptive brachytherapy of iodine-125 prostate implants guided by c-arm cone-beam computed tomography-based dosimetry *Brachytherapy* **6** 231–7

Zhang M, Zaider M, Worman M and Cohen G 2004 On the question of 3D seed reconstruction in prostate brachytherapy: the determination of x-ray source and film locations *Phys. Med. Biol.* **49** N335–45

Zhang Z 1994 Iterative point matching for registration of free-form curves and surfaces *Int. J. Comput. Vis.* **13** 119–52